International Nano Letters (2023) 13:261–272
https://doi.org/10.1007/s40089-023-00402-7

ORIGINAL ARTICLE

Synthesis of cellulose nanofibers from lignocellulosic materials and their photocatalytic dye degradation studies

Prasannakumar Jammapura Kallappa[1] · Prakash Gowdra Kalleshappa[2] · Basavarajappa Bachi Eshwarappa[1] · Suresh Basavarajappa[3] · Virupaxappa S. Betageri[4] · Bharath Kadlera Devendra[5]

Received: 12 August 2022 / Accepted: 9 May 2023 / Published online: 6 June 2023

Abstract

The present research emphasizes lignocellulosic materials like agricultural biomass such as Ragi Stalk also known as Finger Millet Stalk (*Eleusine coracana*), Mango Wood (*Mangifera caesia*), and Groundnut husk (*Arachis hypogaea*) were transformed into cellulose by pretreatment with 5% NaOH and 5% $NaClO_2$ Solution. In addition, the cellulose obtained was transformed into nanocellulose (NC) using acid hydrolysis, ultrasonication, and centrifugation. XRD (X-ray diffraction), SEM (Scanning Electron Microscopy), FTIR (Fourier Transform Infrared Spectroscopy), and TGA/DTA (Thermogravimetry and Differential Thermal Analysis) are used to characterize the nanocellulose that has been synthesized. According to the FTIR findings, the chemical structure of cellulose synthesized from these agricultural biomasses was not affected by the synthetic approach. According to SEM studies, the synthetic procedure employed affects the morphology/surface topology of synthesized nanocellulose. XRD studies reveal the crystalline and semi-crystalline nature of the synthesized nanocellulose. TEM monographs illustrate the morphology and size of the synthesized nanocellulose ranging from 8 to 17 nm. The thermal stability of nanocellulose is revealed by TGA/DTA studies and the obtained nanocellulose shows thermal stability in the range of 270 to 472 °C. A photocatalytic degradation study was carried out for the synthesized NCs like acid hydrolyzed ragi stalk nano cellulose (AH-RSNC), acid hydrolyzed mango wood nanocellulose (AH-MWNC) and acid hydrolyzed groundnut husk nanocellulose (AH-GHNC) for methylene blue (MB) dye under UV light radiation. For the AH-MWHC sample, the dye removal efficiency was obtained at 80%, which indicated an exceptional better dye degradation percentage when compared to the AH-RSNC and AH-GHNC samples. All photocatalytic activity was recorded using a UV–Vis spectrophotometer.

Keywords Ragi Stalk · Mango Wood · Groundnut husk · Acid hydrolysis · Nanocellulose · Dye degradation

✉ Prasannakumar Jammapura Kallappa
prassvin@bietdvg.edu

[1] Department of Chemistry, Research Centre, Bapuji Institute of Engineering and Technology (Affiliated to Visvesvaraya Technological University, Belagavi), Davangere, Karnataka 577004, India

[2] Department of Chemistry, STJPU College, Davangere, Karnataka 577004, India

[3] Department of Civil Engineering, Bapuji Institute of Engineering and Technology (Affiliated to Visvesvaraya Technological University, Belagavi), Davangere, Karnataka 577004, India

[4] Department of Chemistry, Research Centre, G M Institute of Technology (Affiliated to Visvesvaraya Technological University, Belagavi), Davangere, Karnataka 577005, India

[5] Department of Chemistry, M S Ramaiah College of Arts, Science and Commerce, MSR Nagar, MSRIT Post, Bengaluru 560054, India

Introduction

In the preceding years, commendable research has been done on the classification of materials that can be made on a nanoscale and are useful to society [1, 2]. Cellulose is a biopolymer that occurred naturally in plant cells such as wood and cotton and it is a largely available polymer in nature besides the primary ingredient of tree and plant cell walls. The highest cellulose content was found to be in cotton among all the plants and it is about 90% cellulose when compared to wood which contains up to 40–50% cellulose. The bast fibers, such as flax, hemp, or ramie, comprise 70–80% cellulose. Aside from these, cellulose is instituted in a variety of bacterial species, algae, and sea tunicate [3]. Hence, it makes a considerable green nanotechnology material. Any crop containing lignocellulose, which comprises a set of plants, can be used as a primary material for cellulose

synthesis. For nanocellulose synthesis, agricultural biomass is used as starting material. Source materials for nanocellulose extraction from parent cellulose have included olive tree biomass, cotton linter, cereal straws, banana plants, and other materials [4].

Cellulose is a semi-crystalline polycarbohydrate consisting of anhydroglucose units (AGU) linked by chemical β-1,4-glycosidic bonds. Two repeating AGU having a "chair" conformation are shown in Fig. 1. This also includes the carbon atom numbering scheme. There are three hydroxyl functional groups in each of these units one primary and two secondary groups. Owing to the equatorial position of the hydroxyls, the AGU can form internal hydrogen bonds i.e., between the hydrogen atom of the C-3 hydroxyl group of one unit and the atom of the ring oxygen of the adjacent units [5, 6].

Internal hydrogen bonds hinder glucopyranose rings from freely revolving around chemical glycoside bonds, increasing the stiffness of the cellulose chain [7]. As a result of the strong intra and intermolecular hydrogen bonds, crystallites are orderly organized, rigid, and strong cellulose components that are unattainable to water and some chemical reactions. Nanocrystalline amorphous regions with relatively weak hydrogen bonds that contribute to cellulose materials' greater hydrophilicity and accessibility. This biopolymer may establish hydrogen bonds due to the presence of (–OH) hydroxyl groups, making it a strong biopolymer [8]. Cellulose is a semi-crystalline polymer comprising both crystalline and amorphous regions [9]. Nanocellulose is a new shape for this ancient and necessary natural polymer (NC). Over the years, Nanocellulose is an inimitable and natural compound extracted from native cellulose using different extraction methods. Nanocellulose is gaining popularity because of its unique surface shape and chemistry, superior physical and chemical strength, and plenty of hydroxyl groups for modification. Furthermore, its substantial biological features, including biodegradability, biocompatibility, and non-toxicity, as well as its environmental friendliness, make it stand out in nanoengineering and nanomanufacturing. It is used in a variety of applications such as sensing devices, touch feels fabrics [10, 11]. CNCs (cellulose nanocrystals) are natural materials that can be used in the paper and pharmaceutical industries. The various modifications of cellulose nanocrystals have been investigated [12, 13]. Nanocellulose is dispersible in multiple solvents due to a simple chemical modification of the cellulose surface. A strong acid approach is used to hydrolyze the cellulose obtained during the isolation process into nanocellulose [14]. Nanocellulose is used in biomedicine, biocomposite films, supercapacitors, and xerogels and these applications demonstrate the potential of nanotechnology in the synthesis of cellulose from agriculture biomass [15, 16].

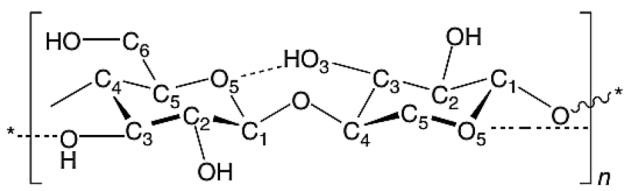

Fig. 1 Repeating unit of cellulose chain

Lignin, hemicellulose, and -cellulose are all known components of lignocellulosic biomass. Nanocellulose is made from α-cellulose, which is made from lignocellulosic material that has been pretreated, and then the lignin was removed using an alkali treatment. The bleaching method removes hemicellulose [17]. The mechanical and chemical techniques can both be used to make nanocellulose from cellulose. The mechanical process involves intensified ultrasonication or high-pressure homogenization and the chemical process involves AH (Acid Hydrolysis), IL (Ionic Liquid), and TEMPO (2, 2, 2, 6,6-tetramethylpiperidine-1-oxyl) [18, 19]. Acid hydrolysis is highly regarded for its ability to hydrolyze cellulose, particularly in the amorphous region. This approach has been used since 1990 and comprises the use of two acids i.e., hydrochloric acid (HCl) and sulphuric acid (H_2SO_4) [20]. When nanocellulose is hydrolyzed in acid, the amorphous zone is preferentially degraded, resulting in cellulose nanocrystals (CNC) with a rod-like shape and crystalline nature retained [21, 22].

Natural nanocelluloses derived from HCl and H_2SO_4 are distinct. This method removes the amorphous region of cellulose, resulting in a structured Cellulose Nano Crystal (CNC) [10, 23]. The NC obtained has high crystallinity and a diameter of less than 20 nm. [24, 25]. For example, nanocellulose synthesized using HCl is deficient in surface charge and subject to electrostatic repulsion. When nanocellulose is produced from H_2SO_4, a colloidal suspension is obtained [26]. When compared to the above-mentioned methods, acid hydrolysis is more feasible in terms of time, cost, and availability of acid. Thus, in the current work, an acid hydrolysis technique was used to synthesize nanocellulose from naturally occurring agricultural bio-waste such as Ragi Stalk, Mango Wood, and groundnut husk, alleviating the strain on the agricultural sector in India to use natural feedstock. Numerous studies have investigated the utilization of mechanical treatment methods such as high-speed blender, high-pressure homogenization, ultrafine grinder, and ball mill to generate nanoscale fibers [27]. This procedure, however, is inefficient at separating hemicellulose, cellulose, and lignin. Sonication and chemical treatment can be used in conjunction to produce pure CNC. There are a number of methods for producing pure cellulose fibers, but sonication has been found to be the easiest of them all. Pure CNCs can be produced using sonication and chemical treatment. To create pure cellulose fibers, the sonication

approach has been found to be the easiest mechanical treatment to use in conjunction with conventional chemical treatments [28, 29].

Biomass-derived from farming the raw materials employed in this research to isolate nanocellulose by acid hydrolysis are Ragi Stalk, Mango Wood, and groundnut husk. The functionality, crystallinity, surface topology, thermal, and photostability of all synthesized nanocellulose were examined using FTIR, XRD, SEM, TEM, TGA/DTG, and UV–Vis Spectra. In this study, synthesized cellulose was examined for the dye degradation application and recorded the sonication effect on the crystalline structure of the nanocellulose which was not emphasized more in previous research. Hence, this method gives a new insight to establish the prospective applications of nanocellulose in the current field of research.

Experimentation

Lignocellulosic materials like agriculture biomass were collected from farmlands in and around Davanagere, Karnataka, India. Sulphuric acid (H_2SO_4), sodium chlorite ($NaClO_2$), acetic acid (CH_3COOH), and sodium hydroxide (NaOH), methylene blue (MB) were purchased from Qualigens and Merck chemicals. All compounds were utilized as such, with purity ranging from 98 to 99%.

Synthesis of cellulose

The procured lignocellulosic materials from agricultural biomass such as Ragi Stalk, Mango Wood, and groundnut husk were separately and thoroughly washed and allowed to expose for sundry for one week then dried in a hot air oven, sieved into fine powder, the powder again dried in hot air oven till it gives constant weight. An appropriate measure of the individual sample was treated with 5% NaOH solution for 3–4 h by maintaining a temperature of 85–110 °C with continuous stirring using a magnetic stirrer. The isolated cellulose residue was filtered until it reached a neutral pH with distilled water. The obtained mass is washed with distilled water and finally with acetone to make it moisture free, dried, and stored for further process.

The bleaching was performed on the material obtained following alkali treatment by treating it with 5% $NaClO_2$ solution for 3–4 h by maintaining acidic pH with glacial acetic acid at 85–110 °C. By washing with distilled water, any remaining residual lignin was eliminated. After that, the filtration of cellulose was done repeatedly with distilled water before being brought to pH = 7. Then this was oven-dried for one day or till it gives constant weight and processed for further preparations. Figure 2 describes the detailed synthesis scheme of acid hydrolysis.

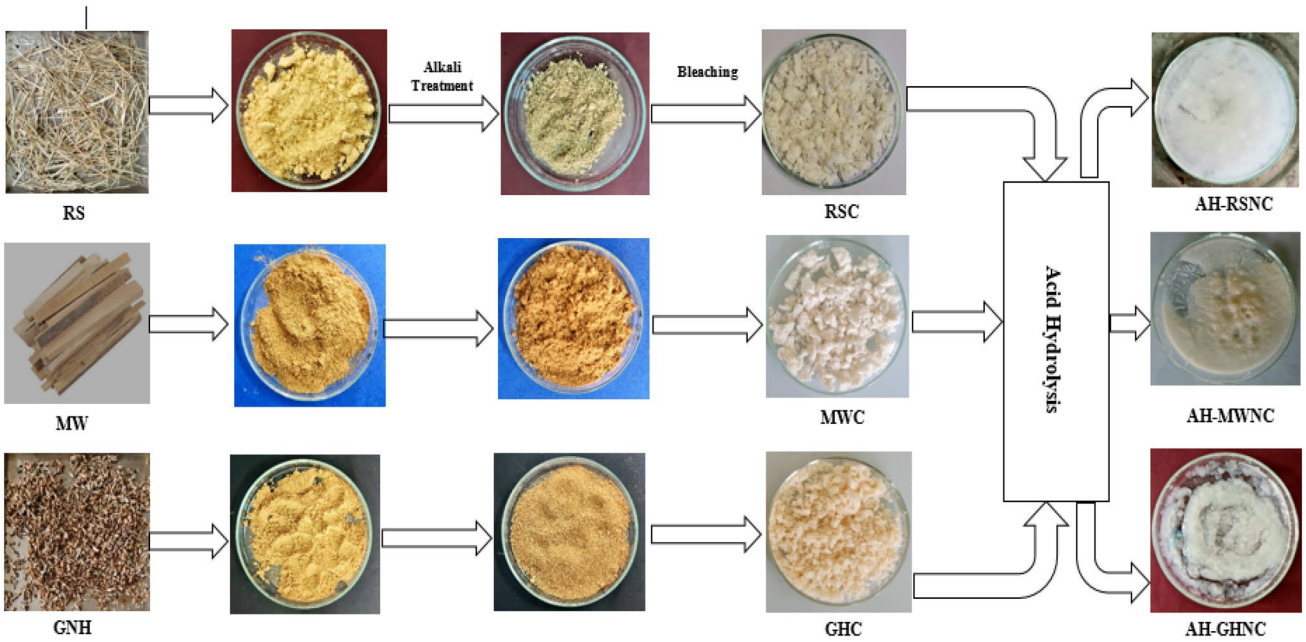

Fig. 2 Acid hydrolysis scheme

Synthesis of nanocellulose from acid hydrolysis

One of the most prominent ways of obtaining nanocellulose from cellulosic materials is acid hydrolysis. The acid may easily hydrolyze the disordered sections of cellulose chains, leaving the orderly parts intact. To break the glycoside bonds in cellulose, a strong acid such as H_2SO_4 or HCl is usually used. Acid hydrolysis is a multi-step process. Under monitored conditions such as concentration of acid, reaction time, temperature, and acid to cellulose ratio [30]. Addition of water to stop the acid hydrolysis process and upon subsequent centrifugation, dialysis to completely remove free acid molecules. Sonication forms a stable nanocellulose suspension followed by drying of the suspension yields solid nanocellulose [31, 32]. This follows the mechanism shown in Fig. 3. To efficiently precede the hydrolysis reaction, water molecules and acid H^+ ions must infiltrate the cellulose fiber throughout this process. Otherwise, only the cellulose surface is affected by hydrolysis. Acid catalyzes the breakdown of long cellulose chains into shorter chain oligomers, which are then degraded by the acid. The hydrolysis of cellulose produces conjugated acid, which begins with an acidic proton and oxygen reaction that links two glucose units together. After the C–O bond is cleaved, the conjugate acid is broken down to the cyclic carbonium ion, which adopts a half-chair conformation. The rapid addition of water causes the release of free sugar and proton. The intermediate carbonium ion forms faster at the end of the polysaccharide chain than it does in the middle [33].

The conventional acid hydrolysis procedure was used to synthesize each sample. 1 g cellulose sample was added with 45 cm^3 H_2SO_4 (55% w/v), and the aliquot mixture was kept for hydrolysis between 40 and 45 °C for about 90 min with continuous stirring. Ice cold deionized water was poured to minimize hydrolysis. The resultant mass obtained was repeatedly washed with distilled water till it reaches neural pH followed by ultrasonication and centrifugation with 4000–5000 rpm for about 30–45 min to obtain AH-RSNC, AH-MWNC, and AH-GHNC. They are kept in the refrigerator until needed.

Photocatalytic experimental setup for dye degradation

Photocatalytic studies were conducted in the core of the cylindrical photoreactor, which comprises a light source [in this case, a 300 W UV light bulb with absorbance at 664 nm (UV–Vis absorption spectra)] surrounded by eight 100 ml quartz reactor tubes and cooling fans. A reaction mixture consisting of a catalytic load of different acid hydrolyzed synthesized of NCs samples, namely AH-RSNC, AH-MWNC, and AH-GHNC. Samples were initially prepared in 100 ml of 5 ppm MB dye. The suspension was swirled for 3 h in the dark. At a steady temperature, the solution was exposed to UV radiation. Every 30 min, samples were taken to determine the percentage of MB degradation. For photocatalytic research, a visible annular photoreactor (Agilent technology Cary-60) was obtained from the scientific company "HEBER" in Chennai, India. In the dark, the MB solution was made using double distilled water. The cylinder reactor is powered by a central light source. The photoreactor is surrounded by eight reactor tubing (each with a capacity of 100 ml) and cooled by fans [34]. Photocatalytic performance was assessed on all of these samples:

$$\% \text{ of degradation} = \left[\left(C_a - C_b\right) / C_a\right] \times 100, \quad (1)$$

where C_a and C_b is initial and final dye concentration, respectively. A variety of characteristics, viz., dye concentration, stability, and pH were used to replicate the study.

Characterization

Thermo Nicolet iS50 was used to record the FTIR of Cellulose, AH-RSNC, AH-MWNC, and AH-GHNC. The samples were pressed into thin pellets after being blended with KBr powder. The wavelength range of the sample was measured from 4000 to 400 cm^{-1}. The Bruker D8 Advance Diffractometer was used to record the XRD data. The peak heights of the crystalline and amorphous zones are measured, and the crystallinity index (CI) was computed using Scherer's

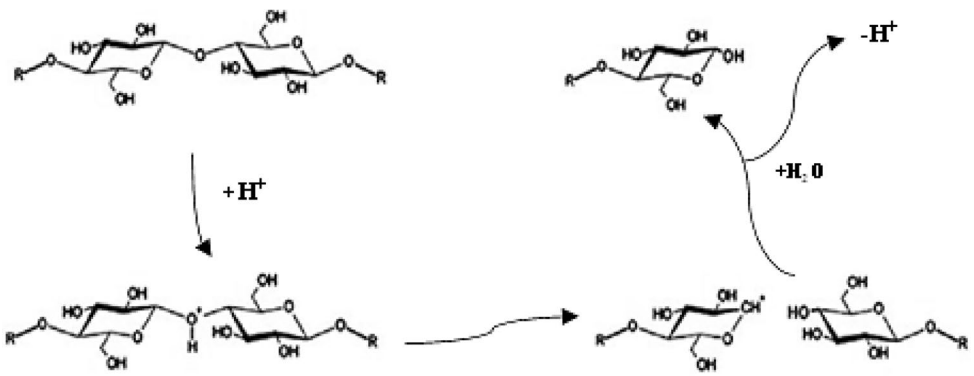

Fig. 3 Acid hydrolysis mechanism

formula, with a step size of 0.02. SEM images were captured with the Jeol 6390LA/OXFORD XMX N instrument, which had an acceleration voltage range of 0.5 to 30 kV. The images were captured using a secondary electron (SE) detector. TEM images were recorded with 200 kV, LaB6 electron gun of point resolution 0.23 nm, lattice resolution 0.14 nm The Perkin Elmer STA 6000 instrument was used for TGA (Thermogravimetric Analysis) and DTA (Differential Thermal Analysis).

Results and discussion

Nanocellulose (NC) is a biopolymer made from biodegradable plant sources that can be produced organically. NC is used in various industries, including packaging, biomedical, and biocomposite preparations. In the present study, Nanocellulose was extracted from agricultural biomasses using the acid hydrolysis method, which included pretreatment with alkali and bleaching. The synthesized NC's chemical group, crystalline nature, structure, and thermal behavior were evaluated using FTIR, XRD, SEM, TEM, and TGA/DTA examinations.

FTIR analysis

The chemical functionality of nanocellulose was examined using FTIR after various chemical treatments. FTIR of Cellulose, AH-RSNC, AH-MWNC, and AH-GHNC in Fig. 4. Peaks can be found in two regions i.e., 2800 to 3500 cm^{-1} in high wavenumbers and 600 to 1800 cm^{-1} in lower wavenumbers. The cellulose peaks can be seen in the FTIR spectral regions shown above.

Broad absorption peaks at 3331.67 to 3334.61 cm^{-1} are characteristic of the O–H stretching vibrations of the hydrogen-bonded hydroxyl groups in cellulose. The C–H and CH_2 groups of cellulose stretching vibrations were ascribed to the peaks at 2893.39 and 2905.06 cm^{-1}. The H–O–H deformation vibration of absorbed water and conjugated C=O stretch vibration are responsible for the peaks at 1637.12 to 1644.34 cm^{-1}. C–H deformation was assigned to the small shoulder peaks vibrations at 1367.83 to 1370.10 cm^{-1} (asymmetric). The O–H association band in cellulose was attributed to the curves at 1104.00 to 1160.40 cm^{-1}. The stretching (C–O) and rocking (C–H) cellulose peaks appeared at 1112 cm^{-1}. The cellulose, peaks at 897.09 cm^{-1} correspond to glycosidic linkage. Out-of-plane bending causes a vibrational band at 557.88 to 664.01 cm^{-1}, which accounts for aromatic C-H vibration in the cellulose range, implying that removal of lignin is not favored by chemical pretreatment. The aforementioned lignin vibrational peaks have decreased slightly in the AH-RSNC, AH-MWNC, and AH-GHNC spectra, showing that remaining lignin is eliminated during acid hydrolysis after Cellulose is dissolved. Chemical and ultrasonic treatments are required to separate lignin from strong hydrogen bonds in AH-RSNC, AH-MWNC, and AH-GHNC. When ultrasonic energy is absorbed by water molecules can cause more efficient cavitation, which embraces the formation, expansion, and disintegration of microscopic gas bubbles. The effect of the ultrasound's hydrodynamic forces on the pulp causes the cellulose fibers to defibrillate. As a result, this method produces aggregated fibrils with a wide width distribution. Some cellulose fibers have been observed to modify their crystalline structure after being subjected to ultrasonic treatment. The shifting of peaks due to transformation of Cellulose-I to Cellulose-II.

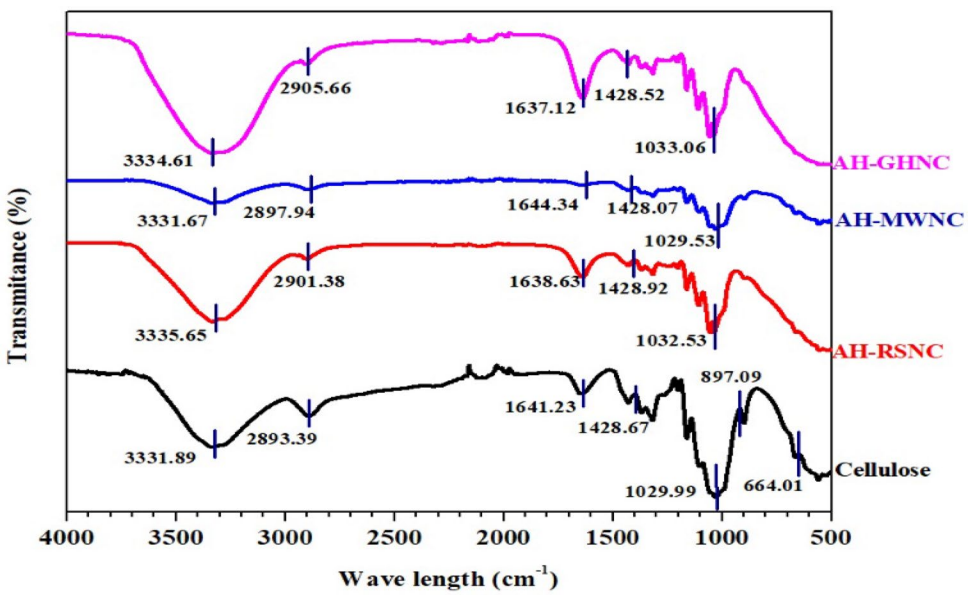

Fig. 4 FTIR of cellulose, AH-RSNC, AH-MWNC, and AH-GHNC

XRD analysis

The crystallinity of nanocellulose elucidates its thermal and mechanical properties, which is a noticeable factor. X-ray diffraction (XRD) patterns are used to study the crystallinity, thermal, and mechanical properties of three synthesized nano celluloses. Cellulose, AH-RSNC, AH-MWNC, and AH-GHNC XRD patterns are shown in Fig. 5, with 2θ values and peak intensities founded on the synthesis method. The cellulose sample exhibits the crystalline peaks at $2\theta = 15.5°$ and 22.23°. AH-RSNC exhibits characteristic peaks at $2\theta = 22.23°$, 29.50°, and 42.00°, while AH-MWNC exhibits peak with 2θ values 15.50°, 22.732°, and 35.00°. The peaks at $2\theta = 22.20°$, 29.17°, and 42.00° are attributed to AH-GHNC. When compared to AH-RSNC, AH-GHNC and Cellulose, AH-MWNC shows strong and intense peaks, indicating better crystallinity. On the other hand, sonication does not affect the cellulose backbone's regular structure. However, AH-RSNC has a significantly wider peak at 29.50°, and AH-GHNC has a little wider peak at 29.17°, Ultrasonic cavitation affects both crystalline and amorphous regions of cellulose, implying that the crystallinity declines and ultrasonic cavitation affect the crystalline and amorphous parts of cellulose simultaneously hinting that crystalline regions are destroyed. As the reaction time is more than 30 min, part of the cellulose crystalline domains of CNCs was removed due to corrosion by sulfuric acid and then resulted in the reduced crystallinity [35, 36]. These findings were also in line with those found by other researchers [37]. But the crystallinity of AH-MWNC remains undisturbed, though ultrasonication had little effect on it. Only amorphous regions or crystalline defect regions are eliminated by this process. As the crystalline regions are more chemically resistant however the decrease in crystallinity observed is mainly due to the breaking of inter and intramolecular hydrogen bonds through acid hydrolysis.

SEM analysis

The synthesized nanocellulose is fibrous, semi-crystalline, and fibrillar, according to the SEM monographs of AH-RSNC, AH-MWNC, and AH-GHNC. The average size of AH- RSNC is between 250 and 300 nm, according to Fig. 6a, b. AH-MWNC has an average between 100 and 150 nm, as shown in Fig. 6c, d, and AH-GHNC has a size of 250–300 nm, as depicted in Fig. 6e, f. All prepared NCs have lengths ranging from a few hundred nm to mμ.

According to these findings, the dimensions of nanocellulose made from Ragi Stalk, Mango Wood, and groundnut husk have different topologies in the nanoscale dimension. As a result, synthetic approaches have an impact on the size distribution and surface morphology, and most of the irregular regions of cellulose are hydrolyzed during the acid hydrolysis process, leaving the fibrous-like NCs behind, resulting in a lower aspect ratio that is ideal for polymer reinforcement. The nanocellulose obtained has a fibrous and fibrillar shape, which facilitates the development of value-added products.

TEM analysis

TEM photos were obtained for the analysis of the internal morphology and structure of the prepared sample. Figure 7 clearly shows that the synthesized sample has nanofibrils and nanofibrous. Nanofibers are distinct and they are arranged in the form of bundles and easily viewable. Across

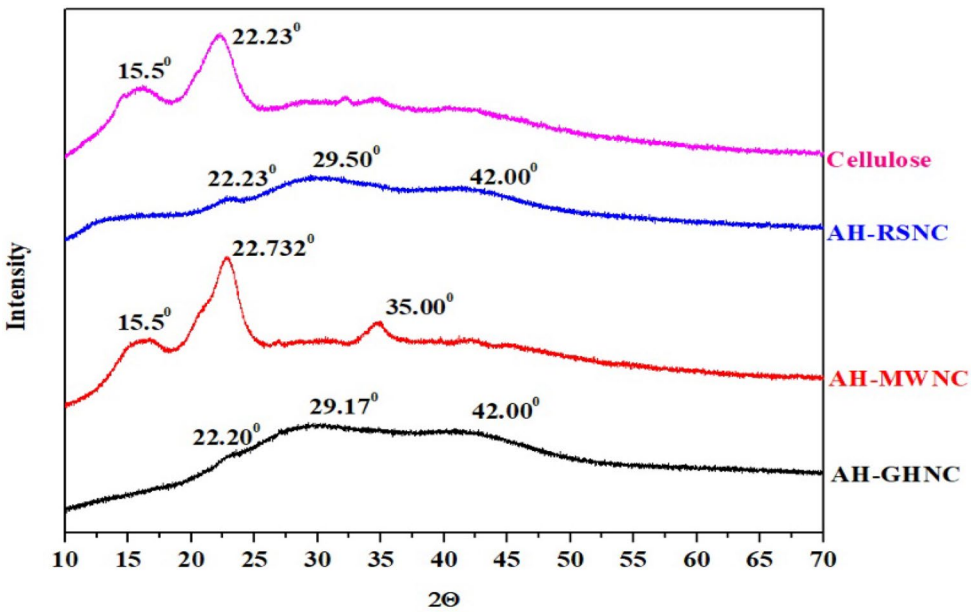

Fig. 5 XRD of, **a** AH-RSNC, **b** AH-MWNC, **c** AH-GHNC and **d** cellulose

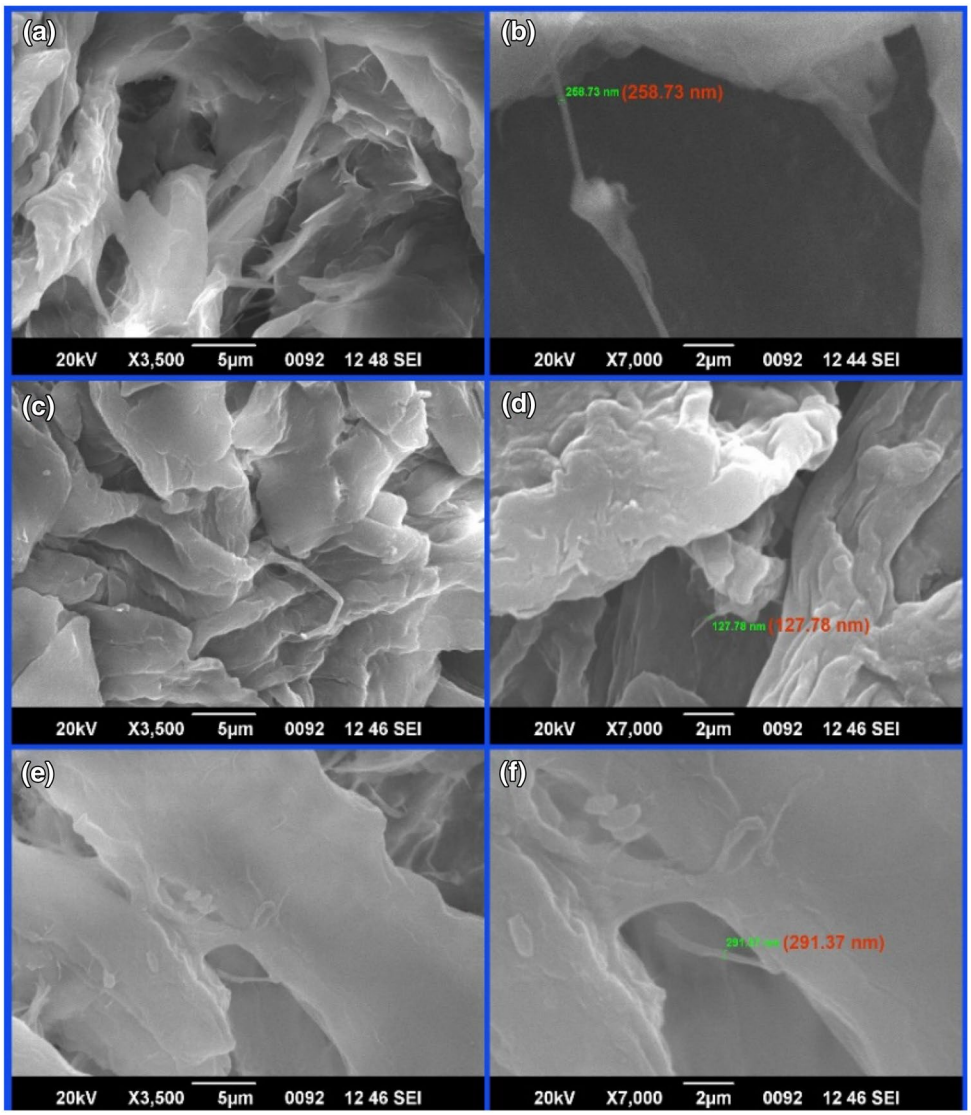

Fig. 6 SEM image of **a**, **b** AH-RSNC, **c**, **d** AH-MWNC, and, **e**, **f** AH-GHNC

all the pictures, even the tendency to agglomerate can also be seen. This tendency can be attributed to the drying conditions during the preparation of samples that involved water evaporation. Figure 7 shows the TEM images of AH-RSNC, AH-MWNC, and AH-GHNC respectively; (a, b) show that AH-RSNC has a long elongated fibrous nature, with an average diameter of 9–14 nm. (c, d) affirms that AH-MWNC has nonfibrillar structures with an average size of 8–15 nm and (e, f) shows that AH-GHNC groups are of nanofibrous structures with diameter between 8 and 17 nm.

TGA/DTA analysis

The thermal stability of the AH-RSNC, AH-MWNC, and AH-GHNC was elucidated using TGA, and the DTA plots are shown in Figs. 8 and 9. The temperatures at which the three types of nanocellulose degrade are as follows: AH-RSNC is 81 °C, AH-MWNC is 75 °C, and AH-GHNC is 127.48 °C. This is shown in the LHS of the DTA curve as small troughs due to the expulsion of the water. AH-RSNC shows loss of weight observed at 250–274 °C and 342.4 °C, AH-MWNC exhibits degradation at 250–327.57 °C and 472.02 °C, whereas AH-GHNC shows a weight loss at 260–310 °C attributes that the nanocellulose degrades primarily as hemicellulose and glycosidic linkages are broken and depolymerized. The temperatures at which the acid begins to degrade are shown as broad troughs. The thermal stability of AH-RSNC, AH-MWNC, and AH-GHNC is impressive. According to these findings, AH-MWNC has the as highest thermal stability up to 472.02 °C due to its high cellulose content and matrix like nanofiber network.

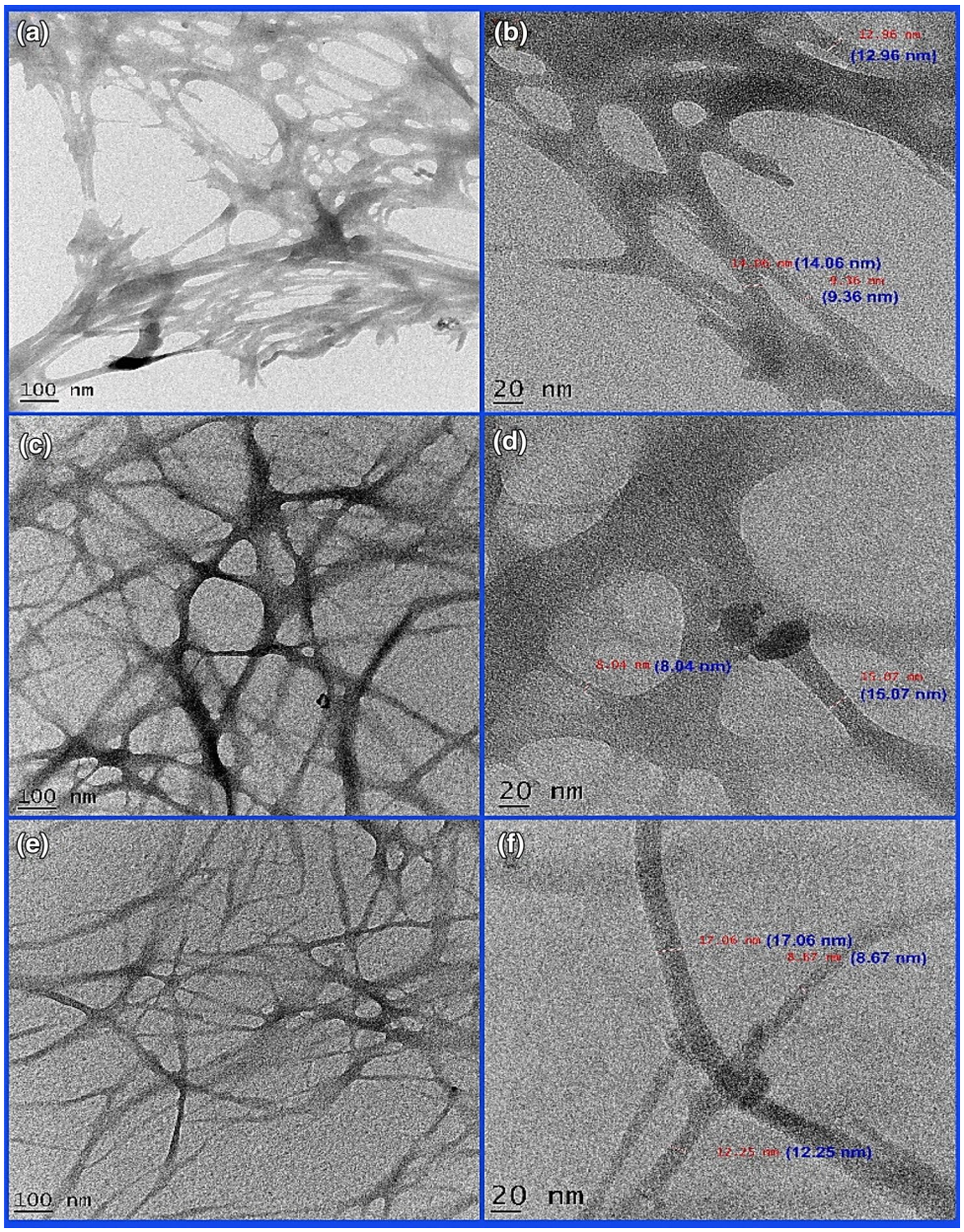

Fig. 7 TEM image of **a**, **b** AH-RSNC, **c**, **d** AH-MWNC and, **e**, **f** AH-GHNC

Photocatalytic dye degradation

The effect of acid hydrolyzed NCs on the photocatalytic degradation of MB dye solution was studied. Methylene blue ($C_{16}H_{18}N_3SCl$) is a cationic heterocyclic aromatic azo-dye, and Fig. 10 depicts its structure. And mechanism of dye degradation in Fig. 11.

Effect of concentration

The dye concentration varies from 10 to 30 ppm and by employing 0.25 g of catalyst for 180 min under visible light irradiation, the effect of dye concentration on degradation (Fig. 12) was observed. The degradation rate and substrate concentrations are directly associated to higher concentrations. The degrading efficiency of all catalysts increased as the concentration decreased. The inaccessibility of photoactive sites at higher concentrations is owing to increased dye molecule adsorption, decreased light penetration due to the screening effect, and dye molecule aggregation at a high rate [38]. For MWNC, RSNC, and GHNC, the maximum degradation was recorded at concentrations ranging from 10 to 30 ppm.

Stability/reusability of the NCs

The recycling of the photocatalyst is a critical component in lowering the cost of materials for industrial

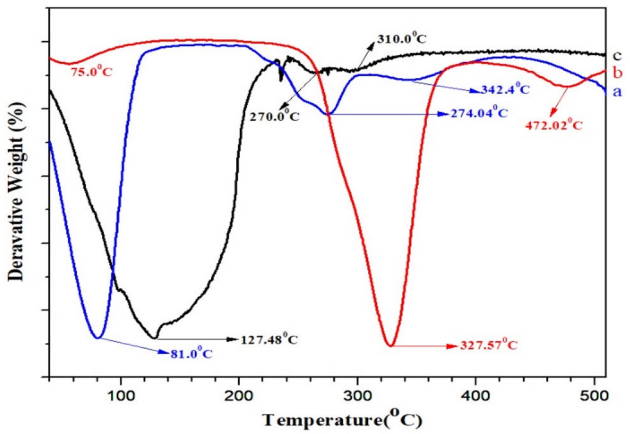

Fig. 8 TGA of **a** AH-RSNC, **b** AH-MWNC and **c** AH-GHNC

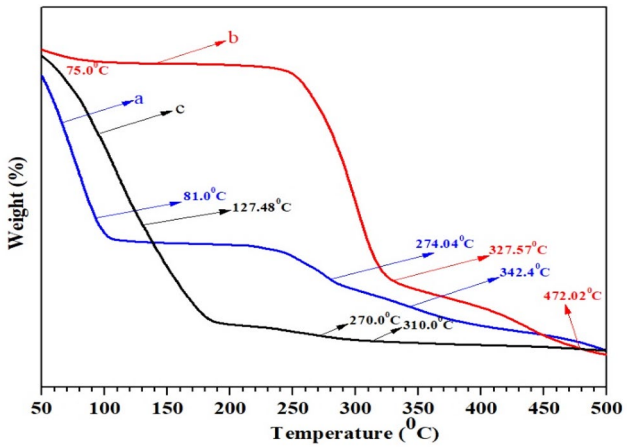

Fig. 9 DTA of **a** AH-RSNC, **b** AH-MWNC and **c** AH-GHNC

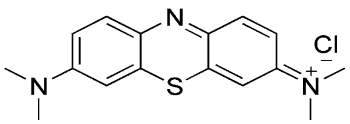

Fig.10 Structure of methylene blue

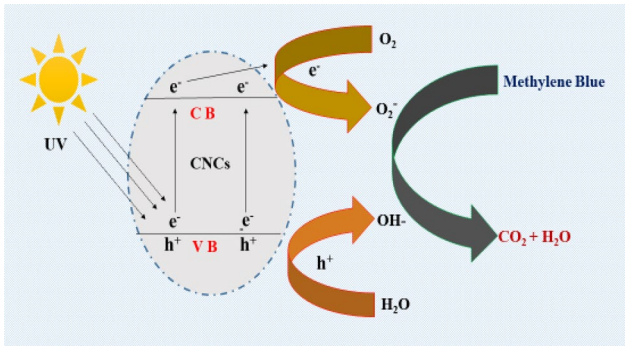

Fig.11 Proposed MB photocatalytic degradation mechanism

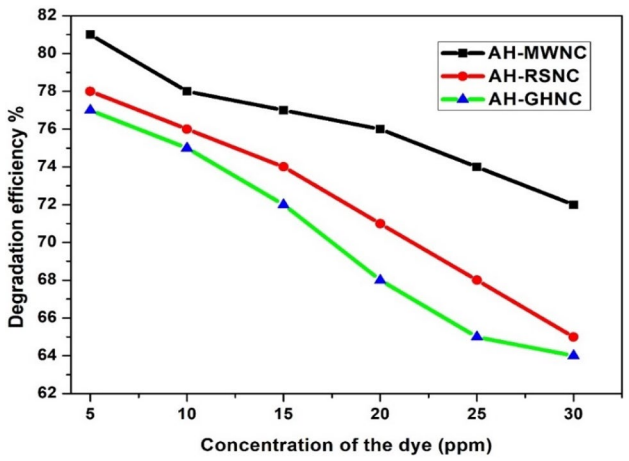

Fig.12 MB degradation efficiency vs. concentration

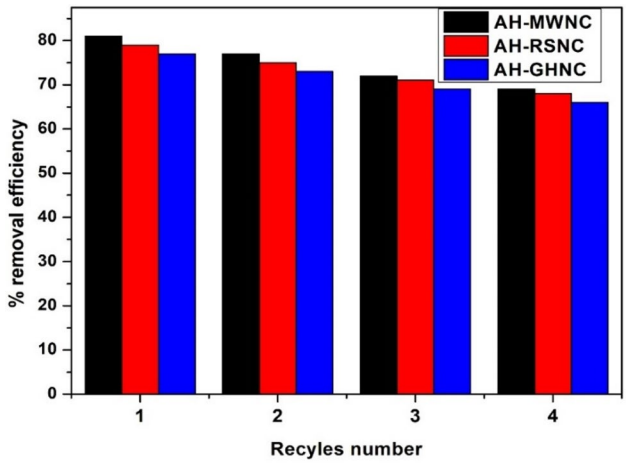

Fig.13 MB degradation efficiency vs. stability/reusability

photocatalytic processes. To analyse the reusability, a photocatalytic recycling study has been done and is represented in Fig. 13. After degradation (cycle 1), all three acid hydrolyzed NCs samples were washed with deionized water to remove the adsorbed dye on the surface of the photocatalyst, followed by drying in the oven to eliminate water molecules. And in the subsequent run, the recovered catalyst was employed again. Four runs of the identical process were completed. After four cycles, the photocatalyst's reusability efficiency dropped from 81% (first cycle) to 67% (4th cycle). There is 14% decrease in photocatalyst activity was observed even after the 4th cycle of degradation [39]. As proved from the previous characteristic data, MWNC shows maximum dye degradation efficiency. The accumulation of external particles on the photocatalyst surface is the main cause of the decrease in the degradation rate [40].

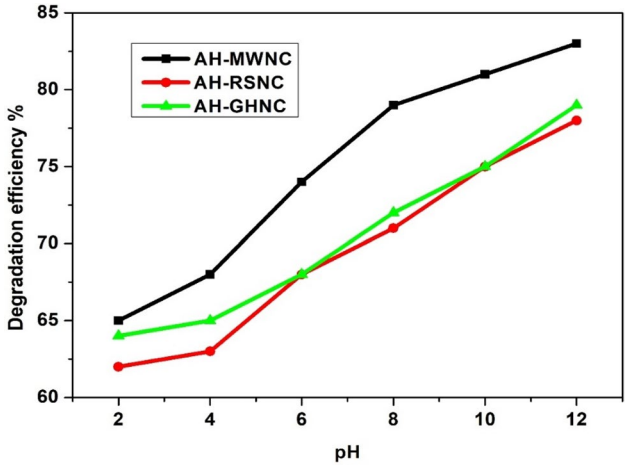

Fig. 14 MB degradation efficiency vs. pH

Effect of pH

The impact of pH on photocatalytic degradation is significant. For the degradation process, the effect of pH was studied over the pH range of 2.0–12.0. A 5 ppm MB dye solution was photo catalytically destroyed in a pH range ranging from 2 to 12 utilizing all three acids catalyzed NCs samples. An increase of photocatalytic activity was recorded with an increase in pH of the solution as seen in Fig. 14. The exterior surface area of NCs samples is positively charged in acidic environments and negatively charged in basic situations. Since MB is a cationic dye and NCs has a negative charge, the electrostatic contact between the negatively charged surface and the cationic MB promotes degradation. The photocatalytic degradation process is accelerated by the greater availability of OH- in the basic medium [41, 42].

Conclusion

In the present work, nanocellulose was extracted from lignocellulosic materials like agricultural biomass Ragi Stalk, Mango Wood Powder, and groundnut husk by acid hydrolysis. Analytical and morphological data were used to characterize the nanocellulose that had been prepared. The impact of synthetic methods on nanocellulose characteristics and morphology was thoroughly examined. According to the FTIR comparison analysis, the synthetic techniques have no detectable effect on the primary functional group areas of cellulose. Acid hydrolysis demonstrates improved crystallinity. The results of SEM show that synthesized nanocellulose comes in a variety of nanoscale forms, including semi-crystalline, fibrous, and fibrillar. The crystallinity and semi-crystalline nature of nano cellulose were depicted by XRD. TGA/DTA analysis shows that the commencement of acid hydrolyzed cellulose degradation is at 75–127 °C, as indicated by the strong troughs in the DTA curve. AH-RSNC. AH-MWNC and AH-GHNC have shown appreciable thermal resistance. The TGA describes acid hydrolyzed AH-MWNC (472.02 °C) has a higher degradation temperature, indicating superior thermal stability. TEM pictures show that synthesized nanocellulose is in the dimension of the nanoscale. The photocatalytic dye degradation studies reveal that these nanocellulose sample shows more efficiency towards the removal of dye. This method clearly displays the nanometer-sized morphology and distribution of synthesized Ragi Stalk, Mango Wood, and groundnut husk. Furthermore, the purpose of this study is to demonstrate a viable application of synthesized cellulose from naturally accessible biomass, thereby addressing India's demand for solid waste management and minimizing chemical waste through a more realistic nanocellulose synthesis process. In our research work, prepared NCs showed an economically viable, and best method for the production of efficient nanomaterials for the removal of organic contaminants and this research will point in a new direction for making better use of nanocellulose derived from agricultural biomass, opening the door to new nanomaterials made from value-added products.

Author contributions All authors contributed to the study conception and design. Material preparation, data collection, and analysis were performed by PJK, PGK, BBE, SB, VSB and BKD The first draft of the manuscript was written by PJK and all authors commented on manuscript. All authors read and approved the final manuscript.

Funding The authors declare that no funds, Grants, or other support were received during the preparation of this manuscript.

Availability of data and materials None.

Declarations

Conflict of interest The authors declare that they have no conflict of interest.

References

1. Nishino, T., Peijs, T.: All-cellulose composites. In: Handbook of Green Materials: 2 Bionanocomposites: Processing, Characterization, and Properties, pp. 201–216 (2014). https://doi.org/10.1142/9789814566469_0028
2. Yamaguchi, A., Sakamoto, H., Kitamura, T., Hashimoto, M., Suye, S.I.: Structure retention of proteins interacting electrostatically with TEMPO-oxidized cellulose nanofiber surface. Colloids Surf. B Biointerfaces **183**, 110392 (2019). https://doi.org/10.1016/j.colsurfb.2019.110392
3. Börjesson, M., Westman, G.: Crystalline nanocellulose—preparation, modification, and properties. Cellul.-Fundam. Aspects Curr. Trends **7** (2015)

4. Espinosa, E., Sánchez, R., Otero, R., Domínguez-Robles, J., Rodríguez, A.: A comparative study of the suitability of different cereal straws for lignocellulose nanofibers isolation. Int. J. Biol. Macromol. **103**, 990–999 (2017). https://doi.org/10.1016/j.ijbiomac.2017.05.156
5. Kargarzadeh, H., Ioelovich, M., Ahmad, I., Thomas, S., Dufresne, A.: Methods for extraction of nanocellulose from various sources. Handb. Nanocellul. Cellul. Nanocompos. **1**, 1–51 (2017)
6. Moon, R.J., Martini, A., Nairn, J., Simonsen, J., Youngblood, J.: Cellulose nanomaterials review: structure, properties and nanocomposites. Chem. Soc. Rev. **40**(7), 3941–3994 (2011)
7. Dufresne, A.: Nanocellulose: From Nature to High Performance Tailored Materials. Walter de Gruyter GmbH & Co KG, Berlin (2017)
8. Chami Khazraji, A., Robert, S.: Interaction effects between cellulose and water in nanocrystalline and amorphous regions: a novel approach using molecular modeling. J. Nanomater. (2013). https://doi.org/10.1155/2013/409676
9. Mansfield, M.L.: Temperature-dependent changes in the structure of the amorphous domains of semicrystalline polymers. Macromolecules **20**(6), 1384–1393 (1987)
10. Habibi, Y., Lucia, L.A., Rojas, O.J.: Cellulose nanocrystals: chemistry, self-assembly, and applications. Chem. Rev. **110**(6), 3479–3500 (2010). https://doi.org/10.1021/cr900339w
11. Faruk, O., Sain, M., Farnood, R., Pan, Y., Xiao, H.: Development of lignin and nanocellulose enhanced bio PU foams for automotive parts. J. Polym. Environ. **22**(3), 279–288 (2014)
12. Pinto, L.O., Bernardes, J.S., Rezende, C.A.: Low-energy preparation of cellulose nanofibers from sugarcane bagasse by modulating the surface charge density. Carbohydr. Polym. **218**, 145–153 (2019). https://doi.org/10.1016/j.carbpol.2019.04.070
13. Ferreira, E.S., Rezende, C.A.: Simple preparation of cellulosic lightweight materials from eucalyptus pulp. ACS Sustain. Chem. Eng. **6**(11), 14365–14373 (2018). https://doi.org/10.1021/acssuschemeng.8b03071
14. Morais, J.P.S., de Freitas Rosa, M., Nascimento, L.D., Do Nascimento, D.M., Cassales, A.R.: Extraction and characterization of nanocellulose structures from raw cotton linter. Carbohydr. Polym. **91**(1), 229–235 (2013). https://doi.org/10.1016/j.carbpol.2012.08.010
15. Fillat, Ú., Wicklein, B., Martín-Sampedro, R., Ibarra, D., Ruiz-Hitzky, E., Valencia, C., Eugenio, M.E.: Assessing cellulose nanofiber production from olive tree pruning residue. Carbohydr. Polym. **179**, 252–261 (2018). https://doi.org/10.1016/j.carbpol.2017.09.072
16. Liu, Y., Sui, Y., Liu, C., Liu, C., Wu, M., Li, B., Li, Y.: A: Physically cross linked polydopamine/nanocellulose hydrogel as potential versatile vehicles for drug delivery and wound healing. Carbohydr. Polym. **188**, 27–36 (2018). https://doi.org/10.1016/j.carbpol.2018.01.093
17. Espinosa, E., Bascón-Villegas, I., Rosal, A., Pérez-Rodríguez, F., Chinga-Carrasco, G., Rodríguez, A.: PVA/(ligno) nanocellulose biocomposite films. Effect of residual lignin content on structural, mechanical, barrier and antioxidant properties. Int. J. Biol. Macromol. **141**, 197–206 (2019). https://doi.org/10.1016/j.ijbiomac.2019.08.262
18. Jagadesh, P., Ramachandramurthy, A., Murugesan, R.: Evaluation of mechanical properties of Sugar Cane Bagasse Ash concrete. Constr. Build. Mater. **176**, 608–617 (2018). https://doi.org/10.1016/j.conbuildmat.2018.05.037
19. Lin, N., Dufresne, A.: Nanocellulose in biomedicine: current status and future prospect. Eur. Polym. J. **59**, 302–325 (2014). https://doi.org/10.1016/j.eurpolymj.2014.07.025
20. Liu, S., Cheng, G., Xiong, Y., Ding, Y., Luo, X.: Adsorption of low concentrations of bromide ions from water by cellulose-based beads modified with TEMPO-mediated oxidation and Fe (III) complexation. J. Hazard. Mater. **384**, 121195 (2020). https://doi.org/10.1016/j.jhazmat.2019.121195
21. Feng, L., Chen, Z.L.: Research progress on dissolution and functional modification of cellulose in ionic liquids. J. Mol. Liq. **142**(1–3), 1–5 (2008)
22. Wulandari, W.T., Rochliadi, A., Arcana, I.M.: Nanocellulose prepared by acid hydrolysis of isolated cellulose from sugarcane bagasse. In: IOP conference series: materials science and engineering, vol. 107, no. 1, p. 012045). IOP Publishing (2016)
23. Mohaiyiddin, M.S., Ong, H.L., Othman, M.B.H., Julkapli, N.M., Villagracia, A.R.C., Md. Akil, H.: Swelling behavior and chemical stability of chitosan/nanocellulose biocomposites. Polym. Compos. **39**, E561–E572 (2018). https://doi.org/10.1002/pc.24712
24. Deepa, B., Abraham, E., Cherian, B.M., Bismarck, A., Blaker, J.J., Pothan, L.A., Kottaisamy, M.: Structure, morphology and thermal characteristics of banana nano fibers obtained by steam explosion. Biores. Technol. **102**(2), 1988–1997 (2011)
25. Jiang, F., Hsieh, Y.L.: Chemically and mechanically isolated nanocellulose and their self-assembled structures. Carbohydr. Polym. **95**(1), 32–40 (2013)
26. Hubbe, M.A., Rojas, O.J., Lucia, L.A., Sain, M.: Cellulosic nanocomposites: a review. BioResources **3**(3), 929–980 (2008)
27. Mahardika, M., Abral, H., Kasim, A., Arief, S., Asrofi, M.: Production of nanocellulose from pineapple leaf fibers via high-shear homogenization and ultrasonication. Fibers **6**(2), 28 (2018). https://doi.org/10.3390/fib6020028
28. Asrofi, M., Abral, H., Kasim, A., Pratoto, A., Mahardika, M., Park, J.W., Kim, H.J.: Isolation of nanocellulose from water hyacinth fiber (WHF) produced via digester-sonication and its characterization. Fibers Polym. **19**(8), 1618–1625 (2018)
29. Wang, Y., Wei, X., Li, J., Wang, F., Wang, Q., Zhang, Y., Kong, L.: Homogeneous isolation of nanocellulose from eucalyptus pulp by high pressure homogenization. Ind. Crops Prod. **104**, 237–241 (2017). https://doi.org/10.1016/j.indcrop.2017.04.032
30. Brinchi, L., Cotana, F., Fortunati, E., Kenny, J.M.: Production of nanocrystalline cellulose from lignocellulosic biomass: technology and applications. Carbohydr. Polym. **94**(1), 154–169 (2013). https://doi.org/10.1016/j.carbpol.2013.01.033
31. Wang, N., Ding, E., Cheng, R.: Thermal degradation behaviors of spherical cellulose nanocrystals with sulfate groups. Polymer **48**(12), 3486–3493 (2007)
32. Dong, X.M., Revol, J.-F., Gray, D.G.: Effect of microcrystallite preparation conditions on the formation of colloid crystals of cellulose. Cellulose **5**(1), 19–32 (1998)
33. Sasmal, S., Mohanty, K.: Pretreatment of lignocellulosic biomass toward biofuel production. In: Biorefining of Biomass to Biofuels, pp. 203–221. Springer, Cham (2018)
34. Gopal, P., Mira, P., Kim, H.Y., Lee, S.Y., Park, S.J.: Electrospun ZnO hybrid nanofibers for photodegradation of wastewater containing organic dyes. A review. J. Ind. Eng. Chem. **21**, 26–35 (2015). https://doi.org/10.1016/j.jiec.2014.03.044
35. Al-Dulaimi, A.A., Wanrosli, W.D.: Isolation and characterization of nanocrystalline cellulose from totally chlorine free oil palm empty fruit bunch pulp. J. Polym. Environ. **25**, 192–202 (2017). https://doi.org/10.1007/s10924-016-0798-z
36. Kargarzadeh, H., Ahmad, I., Abdullah, I., et al.: Effects of hydrolysis conditions on the morphology, crystallinity, and thermal stability of cellulose nanocrystals extracted from kenaf bast fibers. Cellulose **19**, 855–866 (2012). https://doi.org/10.1007/s10570-012-9684-6
37. Kian, L.K., Jawaid, M., Ariffin, H., Karim, Z.: Isolation and characterization of nanocrystalline cellulose from roselle-derived microcrystalline cellulose. Int. J. Biol. Macromol. **114**, 54–63 (2018). https://doi.org/10.1016/j.ijbiomac.2018.03.065
38. Jamal, N., Radhakrishnan, A., Raghavan, R., Bhaskaran, B.: Efficient photocatalytic degradation of organic dye from aqueous

solutions over zinc oxide incorporated nanocellulose under visible light irradiation. Main Group Met. Chem. **43**, 84–91 (2020). https://doi.org/10.1515/mgmc-2020-0009
39. Devendra, B.K., Praveen, B.M., Tripathi, V.S., Nagaraju, G., Nagaraju, D.H., Nayana, K.O.: Highly corrosion resistant platinum–rhodium alloy coating and its photocatalytic activity. Inorg. Chem. Commun. **134**, 109065 (2021). https://doi.org/10.1016/j.inoche.2021.109065
40. Modi, S., Fulekar, M.H.: Synthesis and characterization of zinc oxide nanoparticles and zinc oxide/cellulose nanocrystals nanocomposite for photocatalytic degradation of methylene blue dye under solar light irradiation. Nanotechnol. Environ. Eng. **5**, 18 (2020). https://doi.org/10.1007/s41204-020-00080-2
41. Devendra, B.K., Praveen, B.M., Tripathi, V.S., Nagaraju, G., Nayana, K.O., Nagaraju, D.H.: Platinum coating on SS304: photocatalytic dye degradation application. Iran. J. Sci. Technol. Trans. A Sci. **46**, 37–145 (2022). https://doi.org/10.1007/s40995-021-01250-w
42. Devendra, B.K., Praveen, B.M., Tripathi, V.S., Nagaraju, G., Prasanna, B.M., Shashank, M.: Development of rhodium coatings by electrodeposition for photocatalytic dye. Vacuum **205**, 111460 (2022). https://doi.org/10.1016/j.vacuum.2022.111460